Micropinch formation dynamics in X pinches

Elshafiey, Ahmed Tarief Fawzy
Hammer, Dave
Chalmers, Nate

To be published in: Physical Review E

DOI to publisher's version: 10.1103/PhysRevE.110.L033202

MICROPINCH FORMATION DYNAMICS IN X-PINCHES

A. T. Elshafiey[1,2,*], N. G. Chalmers[2], D. A. Hammer[2]
[1] *Los Alamos National Laboratory, Los Alamos, New Mexico 87544, USA*
[2] *Cornell University, 439 Rhodes Hall, NY, 14853, Ithaca, USA and*
[*] *Corresponding author: ae389@cornell.edu*

High temporal resolution X-ray streak camera studies of micropinch formation in copper (Cu) hybrid X-pinches reveal key plasma conditions. Analysis of Ne-like Cu lines indicate an average electron temperature of about 200 eV and 4.5×10^{28} m^{-3} electron density. The spectra suggest that the electron temperature jumps to about 1 keV, inferred from the continuum and the post-continuum line emission that includes Li-like Cu lines. There was no sign of a rapid temperature change or a substantial surge in radiation emission during the 200 ps pre-continuum X-ray burst, suggesting that the radiative collapse process does not play a major role in micropinch formation. Two-dimensional extended Magnetohydrodynamic (MHD) simulations, coupled to a collisional-radiative spectral analysis code, suggest the significance of the rapid radial implosion of high-temperature, low-density plasma, the axial outflow, and the dynamic plasma pressure in micropinch formation.

Hybrid x-pinches (HXPs) shown in Fig. 1a are primarily used as a backlighter for radiography and absorption spectroscopy for high energy density physics experiments. However, the subject of this study is understanding the formation dynamics of micropinches in HXPs [1–6]. Micropinches are small, dense, short-lived >1 keV plasmas that produce bright bursts of soft x-rays. The HXP consists of a single current-carrying wire connecting conical electrodes that resembles an "X" in a 2D projection. The gap between the two electrodes can be adjusted to control the number of micropinches formed [6]. For radiography, a single micropinch is preferred to avoid overlapping images on time-integrated films of the object under study. Additionally, subsequent micropinches form under different initial conditions than the first one, as the radiation absorbed by the plasma from the first micropinch assists in their formation. Therefore, only the dynamics of the first micropinch are of primary interest in this paper.

HXPs are easier to load than multi-wire X-pinches and produce localized micropinches and X-ray bursts with comparable quality [1]. The experiments were conducted on the XP machine at Cornell University, a pulsed power generator capable of delivering up to 500 kA peak current with a 50 ns 10-90% rise time [7]. The high and rapidly rising current passing through the thin metallic wire induces three main phases. Initially, the wire ablates and ionizes, forming a plasma column that expands rapidly outward due to the temperature and density. As the current continues to increase, the magnetic field induced increases and begins to compress the plasma inwards, what we refer to as the pre-continuum phase. This compression continues until the plasma reaches the stagnation phase, marked by its most compressed state, characterized by the highest temperature and density, and corresponding to the continuum emission phase observed in Fig. 2a and 2c. Following this, the plasma enters an explosive expansion phase, as the magnetic field induced by the driving current can no longer contain or compress the hot, dense plasma, leading to what is described as the post-continuum phase. Detailed K- and L-shell sub-ns spectroscopic studies on hybrid X-pinches and multi-wire X-pinches have been conducted over the past decade in the >1 keV photon energy regime [8–11]. It is important to note that in such photon energy ranges, for the first micropinch formed, no spectral lines are observed prior to micropinch formation, which is the moment that intense X-ray continuum is observed.

A well-known widely used model to explain the extreme parameters reached in micropinches is radiative collapse, a runaway process that assists the magnetic pressure of an imploding Z-pinch by reducing the internal kinetic pressure of the plasma through radiation [12–14]. The process of radiative collapse would be terminated when the plasma becomes optically thick, at which point the radiation energy would be retained in the plasma, increasing its kinetic pressure, and causing the implosion to turn into an explosive expansion that is seen experimentally, as shown in Figures 51 and 52 in Reference [1]. Radiative collapse would be opposed by resistivity-induced heating of the plasma, whether classical or anomalous [15, 16]. Our experimental data demonstrate that radiative collapse does not play a significant role in micropinch formation under the conditions of our experiment. In light of this, we propose an alternative model that more accurately reflects the experimental observations, without relying on the widely accepted but hypothesized radiative collapse model. This model, based entirely on XMHD and independent of radiative losses, provides a comprehensive explanation for micropinch formation.

For the first time in X-pinch research, we successfully captured time-resolved pre-continuum Ne-like L-shell spectra for Cu and Ni wires in the 11-13 Å wavelength range using a streak camera with 17 ps time resolution. This achievement enables a detailed study of the compression phase. The time-resolved L-shell spec-

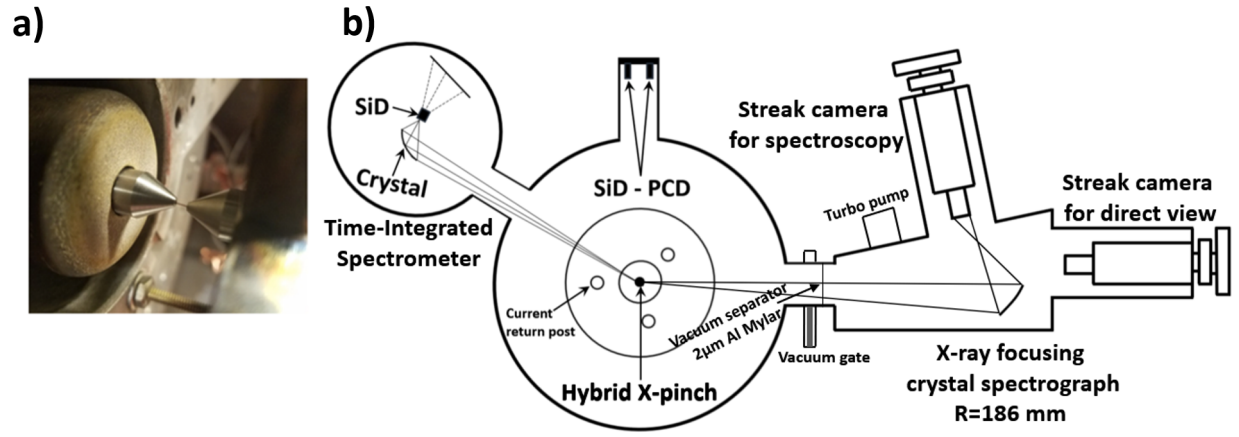

FIG. 1. a) The HXP configuration consisting of two tungsten conical electrodes and a single wire connecting them b) Schematic diagram of the experimental arrangement showing the position of the XRDs, the time-integrated spectrometer, and the streak cameras used.

tra allow us to infer crucial parameters such as the density and temperature of the plasma. Additionally, enable us to observe changes in the intensity of emission which would be indicative of density and temperature changes leading up to micropinch formation. Historically, time-resolved measurements of wavelengths > 10 Å has been challenging, primarily due to low radiation flux before micropinch formation and high absorption by most filters, which are essential for both the functionality and protection of the streak camera, as shown in Fig. 1b. Furthermore, we were able to capture the temporal evolution of this L-shell radiation on an oscilloscope using a novel method described in reference [17]. Our investigation shows that L-shell radiation that emanates from the entire wire persists for as long as 25 ns before the continuum X-ray burst. Subsequently, within a few nanoseconds of micropinch formation, there's a surge of Ne-like line emission that continues up to the moment of intense continuum emission [17]. We deduce that this emission specifically arises from the neck region of the micropinch. PERSEUS, an extended MHD code [18] was used to simulate the experimental load and the output was coupled to SPECT3D [19] to produce synthetic time-resolved radiation spectra and total flux signals. These simulations have been extremely helpful in achieving an understanding of the experimental results.

Given that micropinches are short-lived, extremely dense, and reach very high temperatures, traditional diagnostic techniques such as absorption spectroscopy are not feasible. Radiographing these events is highly challenging due to the rapid dynamics and small spatial scale involved. Similarly, time-integrated emission spectroscopy is unsuitable for diagnosing micropinches, as the point of maximum compression lasts only about 50 ps, while the film used for such measurements would integrate the emission over the entire duration of the current pulse and plasma emission, typically exceeding 100 ns. Therefore, the only viable approach is to use a streak camera to capture the self-emission from the micropinch with high temporal resolution. Time-dependent X-ray spectroscopy was conducted using a Kentech low-magnification streak camera equipped with a LUXEL photocathode made of 3000 Å KBr and 500 Å Al deposited on a 1 μm Lexan substrate. X-rays incident on the 30 mm diameter photocathode produced low-energy electrons that were accelerated and focused onto a 40 mm diameter phosphor screen. An image intensifier based upon a microchannel plate (MCP) was used to amplify the light from the phosphor screen onto a second phosphor screen, which was in contact with TMAX 400 film. For all data presented in this paper, the X-ray streak camera was used at a sweep speed of 172 ps/mm and a total window duration of 6.8 ns. The image intensifier restricted the resolution on the film to 0.1 mm, leading to a temporal resolution of about 17 ps. Using a Plustek OpticFilm scanner, the streak camera images were scanned into a digital format. To account for the nonlinear response of the MCP, film, and scanner, a gamma factor correction was applied to the digitized data. This factor was obtained by comparing the results of a time-integrated spectrometer with an image plate (IP) and the time-resolved spectrometer in static mode with a similar crystal and Bragg angle in the same shot, since the IP is known for its linear response [20].

The streak camera was directly triggered by a brass photoconductive detector sensitive to UV, specifically to bypass the inherent jitter associated with the XP machine. The streak camera trigger timing was then controlled by the length of the 50-ohm cable connecting the brass photodetector to the streak camera sweep unit. With sweep speed 4 (sweep window of 6.8 ns), we were able to capture micropinch spectra with the streak cam-

era from about 70% of the shots. Only the first micropinch is of interest in the present study as subsequent micropinches are formed under varying initial conditions and vary in size and plasma parameters from shot to shot [1, 6, 8, 21]. The streak camera was utilized in conjunction with a spherically bent mica crystal (2d = 19.86 Å) with a 186 mm radius of curvature in a focusing spectrograph with spatial resolution in one dimension (FSSR-1D) [22]. This arrangement eliminates the need for a slit in front of the photocathode. A similar FSSR-1D configuration is used for the time-integrated spectrometer. Mica's first order was utilized to study the Ne-like L-shell emission of Cu in the 11-13 Å regime.

Using the streak camera, we can observe the Ne-like lines before and after the strong Cu continuum, as shown in Fig. 2a. By analyzing the spectral profile as a function of wavelength averaged over the 400 ps indicated by the pre-continuum box in Fig. 2a and utilizing SCRAM, a non-local thermodynamic equilibrium, non-LTE, collisional radiative (CR) model [23], to obtain a matching spectrum, we can estimate the plasma temperature and density. The electron temperature is approximately 200 eV, and the electron density is about $4.5 \times 10^{28}\,\mathrm{m}^{-3}$. A comparison of the theoretical and experimental spectra is shown in Fig. 2b. These results were unexpected, as the temperatures during the continuum emission phase exceed 1 keV, indicating that the temperature jumps abruptly from around 200 eV to over 1 keV. Differences between the theoretical spectrum and the experimental spectrum can be attributed to the presence of density and temperature gradients and the integration over 400 ps, both of which are not taken into account in SCRAM. Importantly, the Ne-like line intensities do not change significantly within the 400 ps interval before the continuum burst, hence there is no evidence of a temperature decline, which would be expected if radiative cooling were a dominant process. Nor is there a significant temperature increase indicated by the emission spectrum that might help explain how the plasma transitions from 200 eV to >1 keV at the moment of continuum emission [4, 7, 8, 10, 11, 14, 21, 24]. The 3C (Ne-like) line for the Cu shots exhibited substantial self-absorption in the pre-continuum phase, which could indicate the presence of temperature and density gradients. However, this self-absorption does not significantly impact the approximate temperature and density obtained from the theoretical model, as the intensity ratios between the different lines are nearly identical, consistent with the methodology used in previous studies to determine plasma density and temperature through line ratios [8].

A 1010 quartz crystal with a 186 mm radius of curvature was used on the streak camera to obtain time-resolved Li-like Cu emission lines in the 5.3-6.7 Å regime. The Li-like L-shell lines appear only after the continuum as shown in Fig. 2c. Before the continuum X-ray burst, the detected radiation was noise-like, which we believe resulted from either energetic electrons accelerated from the anode cone or a low-level emission from a low-density region with an electron temperature greater than 400 eV surrounding the dense plasma core, or both [17]. Given that Ne-like lines occur before the continuum and Li-like Cu lines appear afterward, we can conclude that the temperature jumps from 200 eV to greater than 1 keV within the resolution limits of the streak camera (17 ps).

Using the extended MHD (XMHD) PERSEUS code, rz-cylindrical two-fluid simulations of a 40 μm diameter Cu exploding wire were performed. A sinusoidal current signal with a peak of 350 kA and a rise time of 60 ns (10% to 90%) was used. Due to the lack of radiation cooling rate data for Cu at high densities, we used a modified simple line emission model based on cooling rates for aluminum [25]. This underestimates Cu's radiation losses; the simulation temperatures are expected to be an overestimate. Bremsstrahlung radiation was taken into account in the simulations, but photon reabsorption was not included. The wire's surface was modeled with an axially seeded random roughness of 1 μm, consistent with manufacturing surface tolerances. The simulation is initialized with singly ionized plasma at room temperature and zero current, but no recombination included. For low densities, the ideal gas equation of state with $\gamma = 1.15$ is used, with a transition to the Birch-Murnaghan equation of state with an ambient bulk modulus $k_o = 142$ GPa and a pressure derivative $k^{'}{}_o = 5.25$ for high densities [26]. For temperatures below 1.7 eV, the spitzer resistivity model was utilized, with a transition to the Lee-More-Desjarlais (LMD) electrical conductivity model for higher temperatures. To satisfy the Courant-Friedrichsen-Lewy criterion, a timestep of 10^{-14} s was used along with a cell size of $1\mu m \times 1\mu m$.

The output of the PERSEUS simulation was used as input for SPECT3D, a multi-dimensional collisional-radiative spectral post-processing analysis code. In SPECT3D, we selected the collisional radiative kinetic model and applied the local approximation model, which calculates photoexcitation rates for a given volume element based on the likelihood of photons being able to escape from it. A synthetic detector array was used to observe the radiation emitted and produce synthetic time-resolved spectra. To accelerate the simulation times, a reduced set of Mg, Na, Ne, and F-like line transitions were chosen due to their significant contribution to the radiation at the temperatures and ionization states present before the formation of the micropinch.

As shown in Fig. 3a, 1 ns before the formation of the micropinch, a high-density, cold core with electron temperature below 20 eV was observed. The cold core is surrounded by large gradients in electron temperature and density, with the density increasing towards the axis and the temperature increasing away from the axis by 1-2 orders of magnitude in a few μm. At the boundary of the cold core, at 27.5 ns, there is a $\sim$10 μm diame-

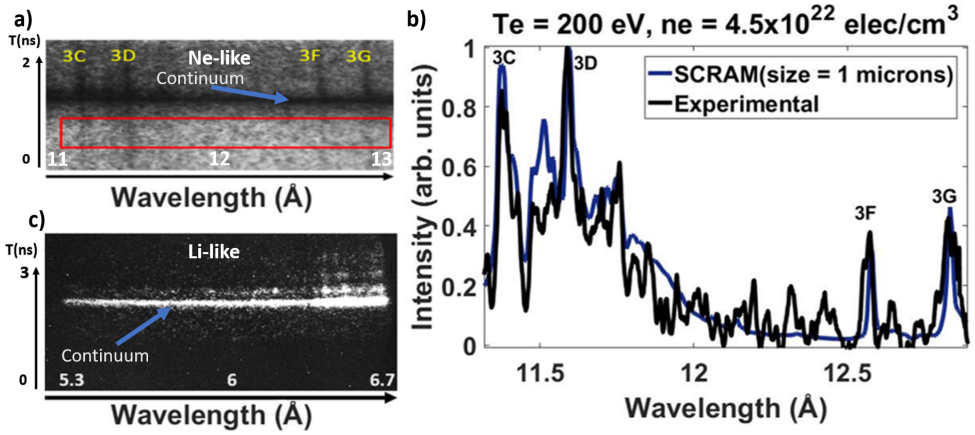

FIG. 2. a) Experimental raw data streak for Ne-like Cu, showing the pre-continuum, 40 ps lasting continuum, and post-continuum radiation. b) An averaged spectral profile, averaged over a 400 ps period, the boxed-portion of the image in a), is shown together with a synthetic spectrum generated by SCRAM based upon the best-fit plasma parameters. c) A time-resolved spectrum of Li-like copper transitions with inverted intensity to show the noise-like radiation prior to the continuum.

ter region of intermediate electron density ($\sim 10^{28}\ m^{-3}$) and electron temperature (>150 eV), which is correlated with the experimental values obtained from the Ne-like Cu emission shown in Fig. 2. Figure 3a suggests that a jet forms within the core as the neck is compressed, resulting in the axial ejection of dense plasma, which enables the imploding micropinch that is about to happen. The mass density distribution snapshots at 27 ns and 27.5 ns show the development of an azimuthally symmetric instability that ultimately leads to the formation of the micropinch. The 27 ns snapshot shows the presence of a neck region with a smaller diameter than the surrounding plasma, indicating the onset of an instability. By 27.5 ns, a subsequent instability can be observed. Although in this instance the micropinch forms at 28.1 ns, experimentally, the micropinch formation is typically observed somewhere between 30 and 35 ns. The early formation of the micropinch observed in the simulation may be attributed to the radiation loss model employed. This model underestimates the radiation losses of copper, resulting in more rapid temperature increases.

The maximum observed current density in the neck region in the simulation was approximately $10^{15} A/m^2$. The neck region had a radius of $\leq 6\,\mu$m and carried a current of 57 kA at 27 ns. By 27.5 ns, the neck radius decreased to $\leq 3\,\mu$m and the current carried within that radius decreased to 26 kA. At 27.8 ns, the neck region had a radius of $\leq 2\,\mu$m and was carrying a current of 13 kA. Finally, at the moment of the micropinch formation, 28.1 ns, the radius was 1 μm and the current carried was 3 kA. The temporal evolution of the neck can be observed by examining a cell in which the micropinch forms, as shown in Fig. 3b. The rapid temperature rise, average temperature, and time scales are all within experimental observations.

The SPECT3D analysis of the cylindrically symmetric

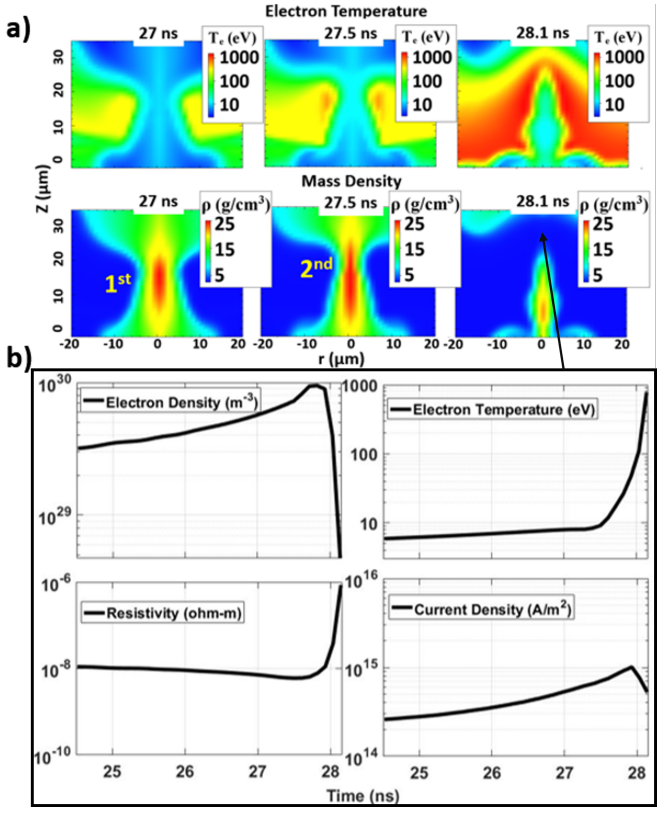

FIG. 3. a) Three temporal simulation snapshots displaying the electron temperature and the mass density at 27 ns, 27.5 ns, and 28.1 ns. The figure shows the cascading sausage instability as seen in the mass density renders, marked as 1st and 2nd. b) Electron density, electron temperature, plasma resistivity, and current density as a function of time in a 1μm cell in the plasma neck at the location indicated by the black arrow.

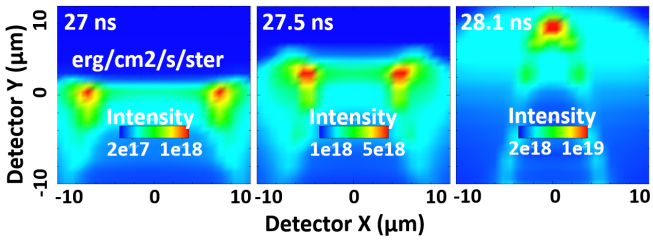

FIG. 4. Synthetic radiation dynamics of the X-ray emitting volume showing the implosion of a radiating annulus on axis, leading to the formation of the micropinch.

PERSEUS data reveals the presence of an annular hot, dense radiating volume surrounding the neck region, as shown in Fig. 4, that would emit Cu L-shell radiation. This annulus has a radius of about 9 μm 1.1 ns before pinch time and decreases to about 5 μm 0.6 ns before pinch time. In the same time interval, the plasma mass within that annulus is reduced due to the axial outflow. At 28.1 ns into the pulse, the annulus implodes to form a 2 μm diameter intense source of radiation on axis, the smallest resolution element in this code run.

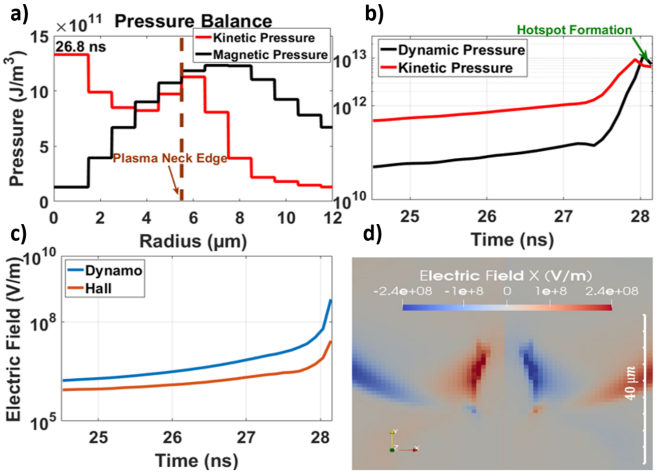

FIG. 5. a) Lineout profiles along the right-side radius of the rz simulation showing the kinetic and magnetic pressure values around the neck region at 26.8 ns, 1.3 ns before the micropinch formation. b) Dynamic, magnetic, and kinetic pressures as a function of time over a cell in the plasma neck. c) Dynamo and hall term electric fields over time over a cell in the plasma neck. d) Electric field in the radial direction across the neck region at 26.8 ns.

Outside of the core / neck region the magnetic pressure is higher than the kinetic pressure due to the low plasma density and the significant amount of current flowing in the coronal plasma. However, within the neck region throughout the entire simulation the kinetic pressure is higher than the magnetic pressure by over an order of magnitude as shown in Fig. 5a. Figure 5d shows the intense electric field around the neck region, which moves closer to the axis and becomes more intense as the neck region shrinks. This electric field can be attributed to the Hall ($\frac{j_z \cdot B_\theta}{e \cdot n_e}$) and dynamo ($v_{ez} \cdot B_\theta$) terms, with the dynamo term playing a more significant role throughout the simulation time, as shown in Fig. 5c. The radial electric field is correlated with the inward radial velocity of the ions in the plasma, leading to an enhancement of the dynamic pressure, which plays a significant role in the formation of the micropinch.

In the face of; the experimental and computational evidence that the micropinch formation is not significantly driven by radiative energy loss for the parameters of our experiment, we now propose an alternative model to explain the sudden emission of the high power radiation pulse observed experimentally. Our model posits that cascading azimuthally symmetric instabilities, specifically the sausage instability, drive the axial outflow of dense, cold plasma from the neck region, while the surrounding low ion density (10^{25} *to* 10^{26} m^{-3}), high temperature (100 eV $< T_e <$ 900 eV) plasma surrounding it is accelerated towards the axis by the magnetic field in the developing instability neck as shown in Fig. 4. The radial electric field formed around the neck region drives an increase in the imploding ion plasma velocity, leading to enhanced dynamic pressure that, in turn, drives enhanced micropinch formation, as shown in Fig. 5b. While a more accurate Cu radiative cooling model within the simulation could assist the magnetic pressure outside of the neck region where the temperature is above 100 eV, our simulations with and without the simple radiation model yielded similar results, suggesting that XMHD alone, i.e., without radiative assistance, can explain the formation of the micropinch adequately at least down to the 2 μm diameter spot size.

To summarize, the combination of experimental and computational results led us to propose a new model to explain the sudden emission of radiation characteristic of a high-temperature plasma; We find compelling experimental evidence that there is not an increase in Cu L-shell radiation in any band we have studied that is sufficient to play a significant role in the final formation phase of the micropinch within the 17 ps time resolution of our X-ray streak camera. That means, at least under the conditions of our 350 kA experiments with Cu wire HXPs, radiative collapse is not playing a major role in the micropinch development up to that moment. The new model is based on the formation of cascading azimuthally symmetric instabilities that lead to the ejection of mass axially as the ultimate micropinch is forming. The micropinch is a result of the high-speed radial implosion of high-temperature, low-density plasma to the axis as the plasma dynamics become dominated by the dynamic pressure of the imploding plasma. The simulation results suggest that the neck region carries only a small fraction of the total current, and therefore remains cold until the arrival of the lower-density, higher-temperature plasma

in a highly compressed form on the axis. This leads to negligible radiative loss from the innermost few μm until the micropinch is fully developed.

ACKNOWLEDGMENTS

We would like to thank Stephanie Hansen from Sandia National Laboratories for her invaluable assistance with the SCRAM software and for generating the synthetic data used in Figure 2b. We are also grateful to Charles Seyler from Cornell University for his assistance with the PERSEUS simulation, and to Reuben Epstein from the Laboratory for Laser Energetics for his assistance with SPECT3D. This research is supported by NNSA funding under the HEDLP Joint Program with DOE FES contract number DE-NA0004027 and partially supported by NNSA SSAP Center Cooperative Agreement DE-NA0003764. Additionally, it was formerly funded by DOE FES grant number DE-SC0018088. This work was performed by the Los Alamos National Laboratory, operated by Triad National Security, LLC for the National Nuclear Security Administration (NNSA) of U.S. Department of Energy (DOE) under contract 89233218CNA000001.

[1] S. A. Pikuz, T. A. Shelkovenko, and D. A. Hammer, "X-pinch. Part I," *Plasma Phys. Rep.*, vol. 41, pp. 291, 2015.

[2] T. A. Shelkovenko, S. A. Pikuz, S. A. Mishin, A. R. Mingaleev, I. N. Tilikin, P. F. Knapp, A. D. Cahill, C. L. Hoyt, and D. A. Hammer, "Title of the article," *Plasma Phys. Rep.*, vol. 38, pp. 359, 2012.

[3] T. A. Shelkovenko, S. A. Pikuz, A. D. Cahill, P. F. Knapp, D. A. Hammer, D. B. Sinars, I. N. Tilikin, and S. N. Mishin, "Hybrid X-pinch with conical electrodes," *Phys. Plasmas*, vol. 17, pp. 112707, 2010.

[4] T. A. Shelkovenko, I. N. Tilikin, G. V. Ivanenkov, W. Stepniewski, A. R. Mingaleev, V. M. Romanova, A. V. Agafonov, A. D. Cahill, C. L. Hoyt, P. A. Gourdain, D. A. Hammer, and S. A. Pikuz, "Dynamics of hybrid X-pinches," *Plasma Phys. Rep.*, vol. 41, pp. 52, 2015.

[5] T. A. Shelkovenko, S. A. Pikuz, C. L. Hoyt, A. D. Cahill, and D. A. Hammer, "Study of new configurations of hybrid X pinches," *IEEE Trans. Plasma Sci.*, vol. 42, pp. 748, 2014.

[6] A. T. Elshafiey, J. Musk, S. A. Pikuz, T. A. Shelkovenko, and D. A. Hammer, "Studies and optimization of hybrid X-pinches," *Plasma Research Express*, vol. 3, 015004, 2021.

[7] S. A. Pikuz, T. A. Shelkovenko, and D. A. Hammer, "X-pinch. Part II," *Plasma Physics Reports*, vol. 41, pp. 445, 2015.

[8] D. B. Sinars, S. A. Pikuz, T. A. Shelkovenko, K. M. Chandler, D. A. Hammer, and J. P. Apruzese, "Time-resolved spectroscopy of Al, Ti, and Mo X pinch radiation using an X-ray streak camera," *J. Quant. Spectrsoc. Radiat. Transf*, vol. 78, pp. 61, 2003.

[9] S. B. Hansen, *Development and Application of L-Shell Spectroscopic Modeling for Plasma Diagnostics*, Ph.D. thesis, University of Nevada, Reno, 2003.

[10] T. A. Shelkovenko, S. A. Pikuz, I. N. Tilikin, A. Elshafiey, and D. A. Hammer, "Time-Resolved Investigation of Subnanosecond Radiation from Al Wire Hybrid X Pinches," *Phys. Rev. E*, vol. 102, pp. 063208, 2020.

[11] T. A. Shelkovenko, S. A. Pikuz, I. Yu, D. B. Skobelev, K. M. Sinars, M. D. Chandler, D. A. Mitchell, and Hammer, "X-pinch plasma conditions from time resolved x-ray spectroscopy," *Review of Scientific Instruments*, vol. 74, pp. 1958, 2003.

[12] K. N. Koshelev and N. R. Pereira, "Plasma points and radiative collapse in vacuum sparks," *Journal of Applied Physics*, vol. 69, pp. 21, 1991.

[13] J. W. Shearer, "Contraction of z pinches actuated by radiation losses," *Phys. Fluids*, vol. 19, pp. 1426, 1976.

[14] S. A. Pikuz, D. B. Sinars, T. A. Shelkovenko, K. M. Chandler, D. A. Hammer, G. V. Ivanenkov, W. Stepniewski, and I. Y. Skobelev, "High energy density z-pinch plasma conditions with picosecond time resolution," *Phys Rev Lett*, vol. 89, pp. 035003, 2002.

[15] V. I. Oreshkin, E. V. Oreshkin, S. A. Chaikovsky, and A. P. Artyomov, "Coulomb explosion of "hot spot," *Phys. Plasmas*, vol. 23, pp. 92701, 2016.

[16] A. E. Robson, "Anomalous resistivity and the Pease-Braginskii current in a z pinch," *Phys. Rev. Lett*, vol. 63, pp. 2816, 1989.

[17] A. T. Elshafiey, N. G. Chalmers, S. A. Pikuz, T. A. Shelkovenko, and D. A. Hammer, "Sub-nanosecond time-resolved radiation measurement using x-ray focusing crystal spectrometers," *Review of Scientific Instruments*, vol. 94, pp. 083508, 2023.

[18] N. D. Hamlin and C. E. Seyler, "Relativistic modeling capabilities in perseus extended-mhd simulation code for hed plasmas," *IEEE Transactions on Plasma Science*, vol. 44, pp. 1112, 2016.

[19] J. J. Macfarlane, I. E. Golovkin, P. Wang, P. R. Woodruff, and N. A. Pereyra, "SPECT3D - A multi-dimensional collisional-radiative code for generating diagnostic signatures based on hydrodynamics and PIC simulation output," *High Energy Density Physics*, vol. 3, pp. 181, 2007.

[20] K. Zeil, S. D. Kraft, A. Jochmann, F. Kroll, W. Jahr, U. Schramm, L. Karsch, J. Pawelke, B. Hidding, and G. Pretzler, "Absolute response of Fuji imaging plate detectors to picosecond-electron bunches," *Review of Scientific Instruments*, vol. 81, pp. 13307, 2010.

[21] S. A. Pikuz, D. B. Sinars, and T. A. Shelkovenko, "Time-resolved X-ray spectroscopy of hot spots in an X-pinch," *Jetp Lett*, vol. 76, pp. 490, 2002.

[22] T. A. Shelkovenko, D. B. Sinars, S. A. Pikuz, and D. A. Hammer, "Radiographic and spectroscopic studies of X-pinch plasma implosion dynamics and x-ray burst emission characteristics," *Physics of Plasmas*, vol. 8, pp. 1305, 2001.

[23] S. Hansen, J. Bauche, C. Bauche-Arnoult, and M. Gu, "Hybrid atomic models for spectroscopic plasma diagnostics," *High Energy Density Phys*, vol. 3, pp. 109, 2007.

[24] M. Mitchell, *X-Pinch Plasma Dynamics Studied with High Temporal Resolution Diagnostics*, Ph.d. dissertation, Cornell University, 2007.

[25] F. Suzuki-Vidal, S. V. Lebedev, A. Ciardi, L. A. Pickworth, R. Rodriguez, J. M. Gil, G. Espinosa, P. Harti-

gan, G. F. Swadling, J. Skidmore, G. N. Hall, M. Bennett, S. N. Bland, G. Burdiak, P. de Grouchy, J. Music, L. Suttle, E. Hansen, and A. Frank, "Bow shock fragmentation driven by a thermal instability in laboratory astrophysics experiments," *The Astrophysical Journal*, vol. 815, pp. 96, 2015.

[26] D. Grady, "Equation of state for solids," *AIP Conference Proceedings*, vol. 1426, pp. 800, 2012.